Science Advances
AAAS

advances.sciencemag.org/cgi/content/full/4/9/eaat9722/DC1

Supplementary Materials for

Pulling apart photoexcited electrons by photoinducing an in-plane surface electric field

E Laine Wong, Andrew J. Winchester, Vivek Pareek, Julien Madéo, Michael K. L. Man, Keshav M. Dani*

*Corresponding author. Email: kmdani@oist.jp

Published 7 September 2018, *Sci. Adv.* **4**, eaat9722 (2018)
DOI: 10.1126/sciadv.aat9722

The PDF file includes:

Other Supplementary Material for this manuscript includes the following:

(available at advances.sciencemag.org/cgi/content/full/4/9/eaat9722/DC1)

SUPPLEMENTARY MATERIALS

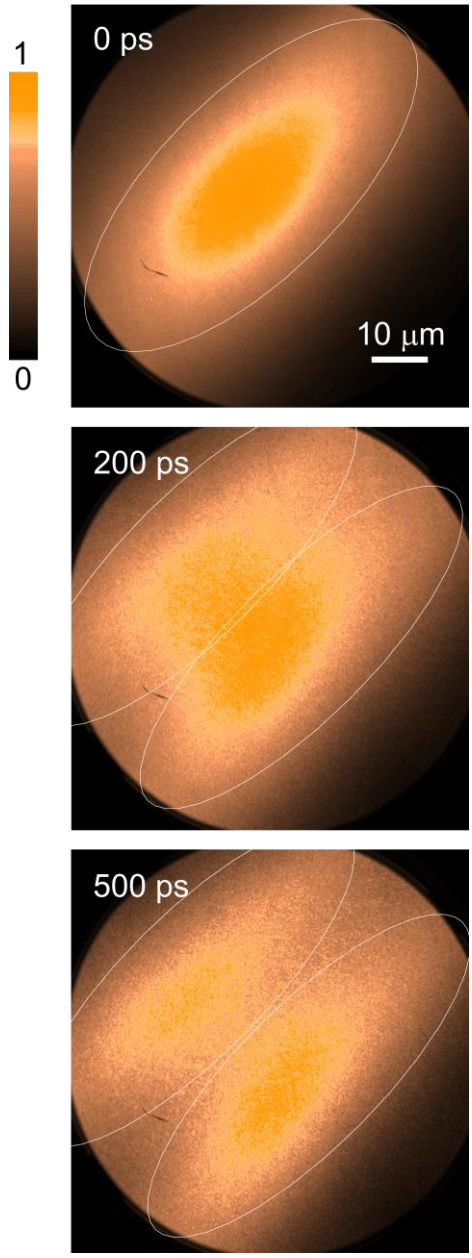

Fig. S1. 2D images showing the separation of the photoexcited electrons at the photoexcited carrier density of 2.1 × 10^{19} cm^{-3}. The snapshots show the normalized spatial distribution of the photoexcited electrons at three different time delays after photoexcitation i.e. 0 ps, +200 ps, and +500 ps. The white elliptical lines mark the FWHM of the distribution(s). At 0 ps, the photoexcited electrons inherits the elliptical profile of the photoexciting beam resulting in a stronger lateral electric field along the short axis of the elliptical profile. Due to the anisotropic electric field, the electron distribution profile starts to separate along the short axis of the ellipse at +200 ps and eventually split into two distinct distributions at +500 ps. The white elliptical

lines at +500 ps show that the separation between the two peaks of the separated distributions is greater than the FWHM of the distributions.

Section S1. Partial screening of the built-in surface space charge field

At thermal equilibrium, the positively charged surface states of p-type GaAs is balanced by a negatively charged depletion region in the bulk leading to the buildup of a built-in surface space charge field (Fig. S2A). Upon photoexcitation, the photoexcited electrons are pulled towards the positively charged surface while the photoexcited holes are pulled towards the negatively charged bulk. The separation of the photoexcited electrons and holes leads to the buildup of a reverse electric field and partially screens the built-in surface field. As a result, it leaves behind a slightly less positively charged surface and a correspondingly less negatively charged bulk (Fig. S2B).

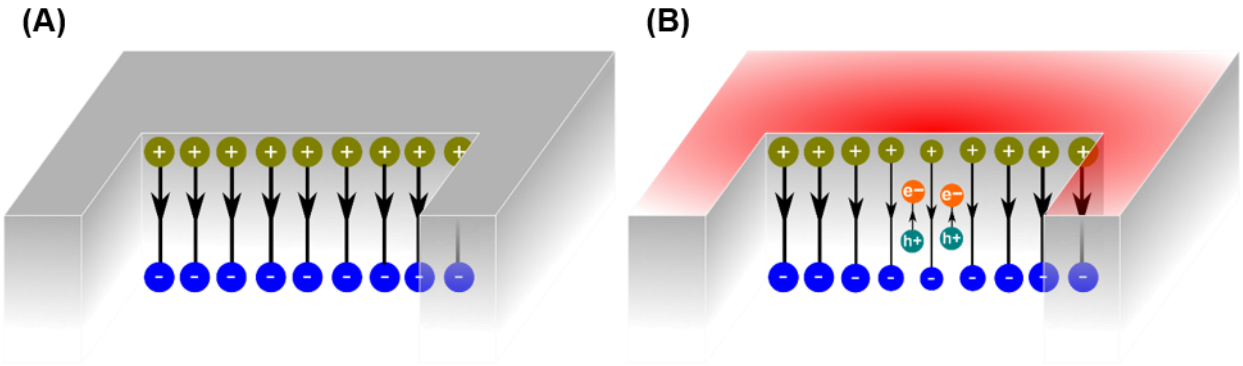

Fig. S2. Distribution of dipoles (A) before and (B) after photoexcitation.

To demonstrate the screening dynamics of the built-in surface field as a function of the photoexcited carrier density, we measured the time-delayed photoemission intensity of a 4 μm x 4 μm spot at the center of the photoexcitation beam where the photoexcitation density is relatively homogeneous (Fig. S3A). At a relatively low carrier density of 1.4 x 10^{18} cm^{-3}, the photoemission intensity continues to increase up to +10 ps after the instant of photoexcitation due to the vertical transport of the photoexcited electrons from the bulk to the sample surface. As the photoexcited carrier density increases, the built-in surface field becomes increasingly screened resulting in less photoexcited electrons reaching the sample surface. At sufficiently high carrier density (1.1 x 10^{19} cm^{-3}), the built-in field is fully screened and the surface bands completely flattened resulting in the absence of vertical transport of electrons to the surface, as evidenced by the lack of increase in the photoemission intensity. The photoemission intensity instead shows a monotonous decrease as the photoexcited electrons decay and recombine over time. To explain the fast drop in the photoemission intensity within the first few hundreds of femtoseconds, the rate of decrease in the intensity ($-\frac{\Delta Intensity}{\Delta delay}$) is plotted as a function of the

carrier density, n (Fig. S4). A good agreement between the $-\frac{\Delta Intensity}{\Delta delay}$ plot with the n^3 curve indicates the origin of the fast drop to be likely due to Auger recombination (*36*).

To demonstrate the inhomogeneous screening of the built-in surface field now as a function of the intensity variation within the Gaussian photoexcitation profile, we measured the time-delayed photoemission intensity at three different spatial locations within the photoexcitation spot (Fig. S3B). The PEEM image (inset in the upper panel of Fig. S3B) indicates the three spatial locations within the photoexcitation spot. At the center of the spot where the local photoexcitation intensity is the highest, the rise in the photoemission intensity is smaller as the largely screened built-in field results in less electrons reaching the sample surface. Near the FWHM boundary where the local photoexcitation intensity is lower, the rise in the photoemission intensity is much larger as the built-in field is partially screened and hence a larger density of the photoexcited electrons drift to the sample surface.

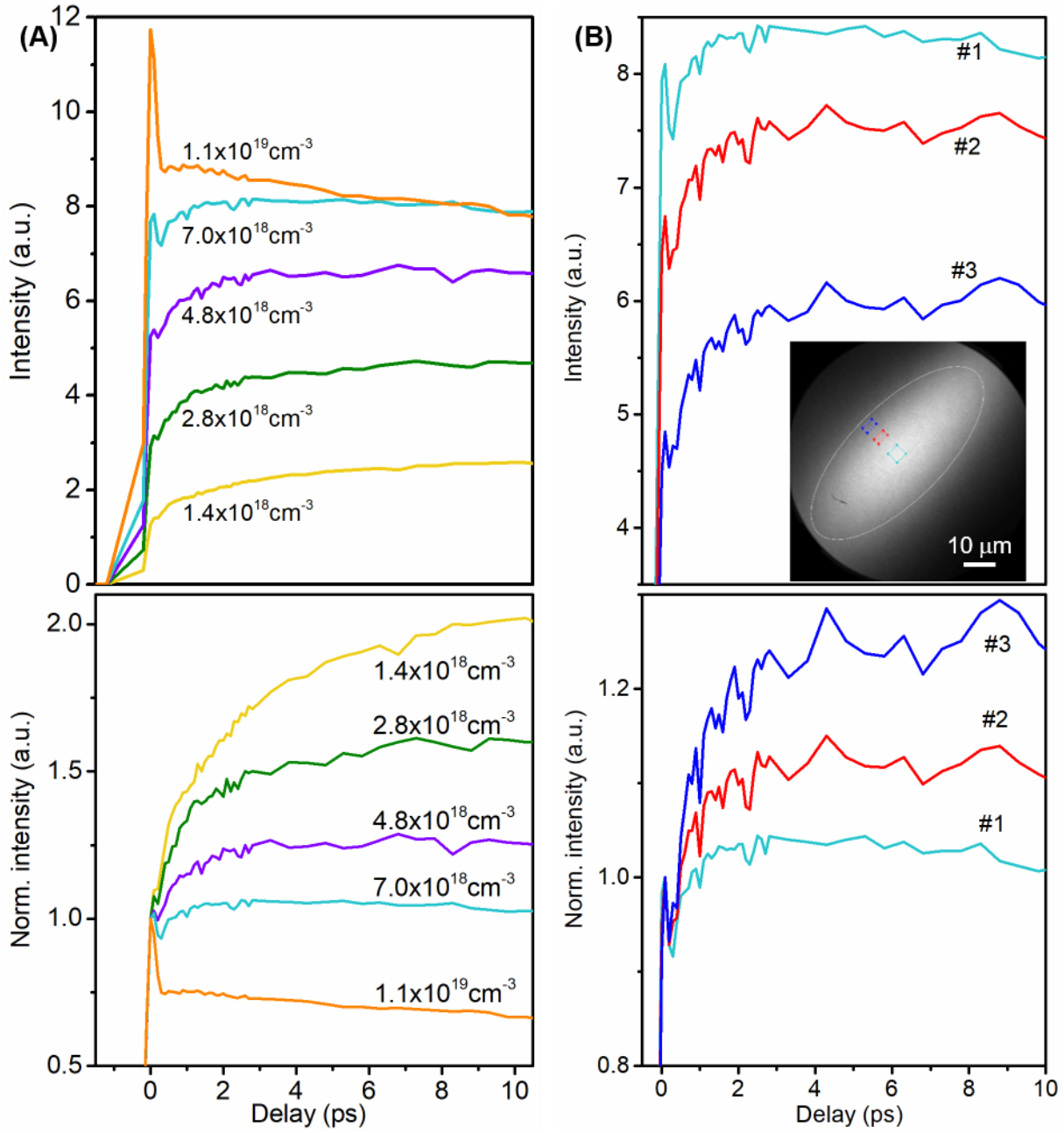

Fig. S3. Partial screening of the built-in surface field. (**A**) **Upper panel**: Time-delayed photoemission intensity as a function of the photoexcited carrier density, measured at a 4 μm x 4 μm spot at the center of the Gaussian photoexcitation spot. **Lower panel**: Normalized time-delayed photoemission intensity to highlight the increase in the photoemission intensity after 0 ps due to the vertical transport of the photoexcited electrons to the sample surface. (**B**) **Upper panel**: Time-delayed photoemission intensity at three different spatial locations relative to the Gaussian photoexcitation spot as demarcated in the inset PEEM image. The measurement spot at the center is 4 μm x 4 μm while the two spots further away is 2 μm x 4 μm to maintain sufficient signal-to-noise ratio while diminishing the averaging effect across a range of local

photoexcitation density at the slope of the Gaussian profile. The white ellipse marks the FWHM of the photoexcited electron distribution. A greater increase in the photoemission intensity is measured at the spot near the FWHM boundary due to lesser screening of the built-in field than at the center of the photoexcitation spot. **Lower panel**: Normalized time-delayed photoemission intensity to highlight the increase in the photoemission intensity after 0 ps.

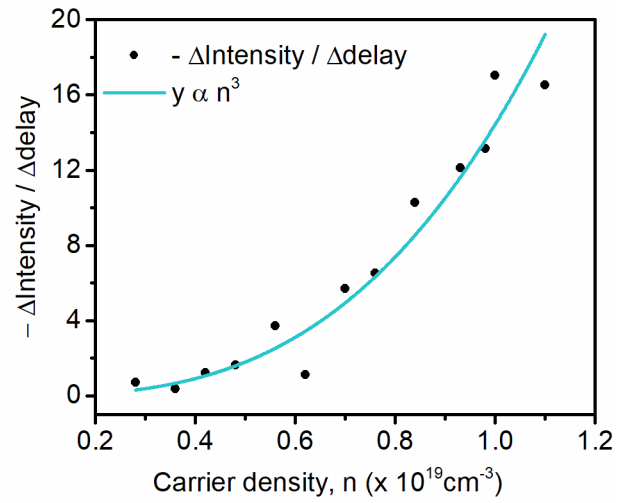

Fig. S4. Origin of the initial fast drop in the photoemission intensity. The rate of decrease in the intensity shows a good agreement with the n^3 curve indicating the origin of the fast drop to be likely due to Auger recombination.

Section S2. Formation of lateral electric field

The inhomogeneous distribution of the photoexcited carriers leads to a spatially nonuniform screening of the built-in field as demonstrated in Fig. S3B. The gradient of the unscreened positive surface charges gives rise to an in-plane surface electric field that acts upon the photoexcited electrons, pulling them apart as observed in Fig. 2B.

To verify that the spatially nonuniform screening of the built-in field will indeed lead to the buildup of a lateral electric field along the surface, we modeled the surface space charge field as a layer of dipoles separated by the width of the depletion region, w (Fig. S5A). We note that in general, the negative charges are evenly distributed throughout the depletion region. However, to calculate the electric field at the surface due to these evenly distributed negative charges in the depletion region, we use an equivalent plane of negative charges at a fixed depth from the surface, which gives the same result. The photoexcited electrons close to the center of the photoexcitation spot experience a lateral pull outward, towards the unscreened positive surface charges while the negative charges deeper within repel the photoexcited electrons pushing them in the opposite x-direction (Fig. S5B). Due to the longer distance, the photoelectrons closer to the

positive surface charges in the +x direction will experience a net attractive pull towards the +x direction, and vice versa for the electrons closer to the positive surface charges in the –x direction. As such, the surface electric field due to these positive surface charges is

$$E_+(a) = -\frac{q}{2\pi\varepsilon_0}\int \sigma[1 - e^{\frac{-x^2}{2c^2}}]\frac{dx}{(x-a)}$$

where σ is the surface charge density. Correspondingly, the surface electric field in the x-direction due to the negative charges at z = -w is

$$E_-(a) = \frac{q}{2\pi\varepsilon_0}\int \sigma[1 - e^{\frac{-x^2}{2c^2}}]\frac{(x-a)dx}{(x-a)^2 + w^2}$$

and the resultant surface electric field due to this layer of dipoles is as shown in Fig. S5C. With this surface electric field, we then modeled the lateral transport of the photoelectrons at the surface with the following drift-diffusion equation

$$\frac{\partial N(x,t)}{\partial t} = \mathrm{D}\nabla^2 N(x,t) + \mu E(x)\nabla N(x,t) - \frac{N(x,t)}{\tau}$$

where N is the electron density, D is the diffusion coefficient, μ is the electron mobility, and τ is the recombination rate. Here, we use D=85 $cm^2 s^{-1}$, μ=3300 $cm^2 V^{-1} s^{-1}$, and τ=500 ps as fitting parameters. Our model allows us to reproduce qualitatively the photoexcited electron distribution profile as shown in Fig. 4D. In order to extract relevant physical parameters from the data, more rigorous theoretical modelling would be necessary, which also accounts for effects like the attraction between the photoelectrons and the photoholes.

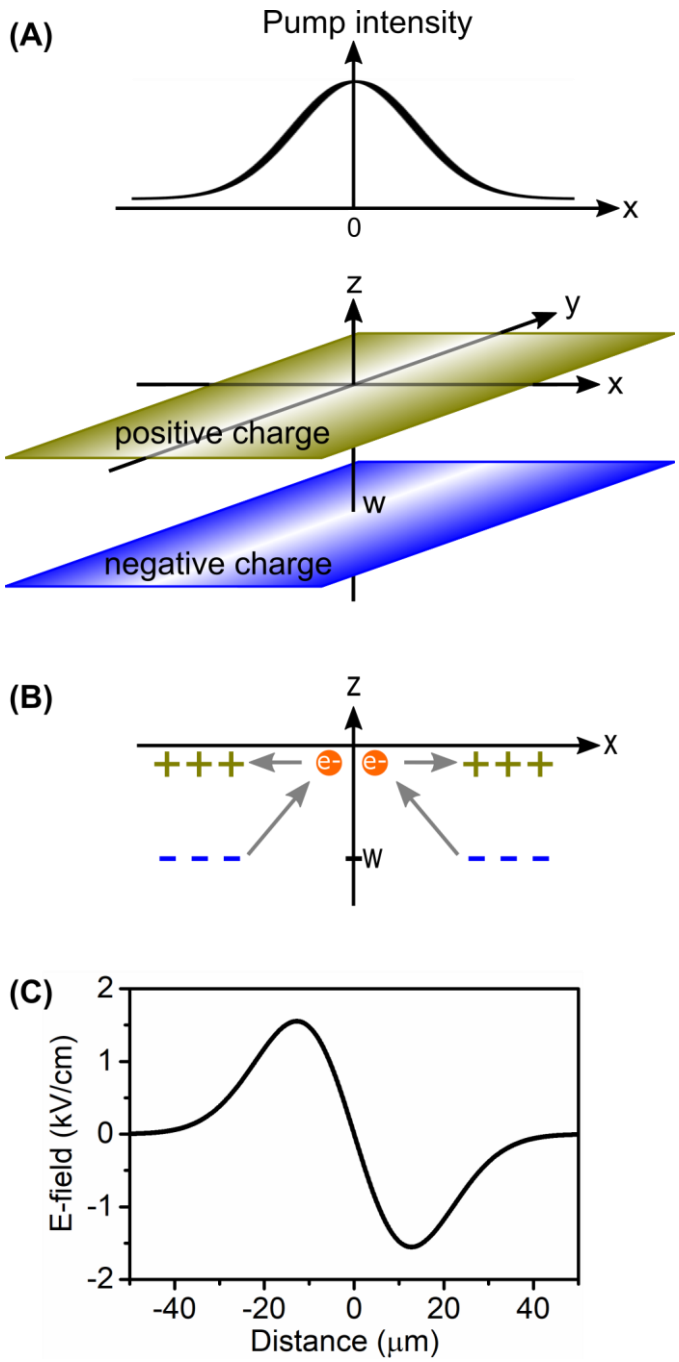

Fig. S5. Formation of the in-plane electric field. (**A**) The nonuniform screening of the surface space charge field due to the photoexcitation pulse is modelled as a layer of dipoles. (**B**) The layer of positive charges (dark yellow plus sign) along the surface attracts the surface photoexcited electrons (orange balls) while the layer of negative charges (blue minus sign) in the depletion region repels the surface photoexcited electrons in the opposite x-direction. (**C**) The nontrivial spatially varying in-plane electric field that arises from the unscreened dipoles.

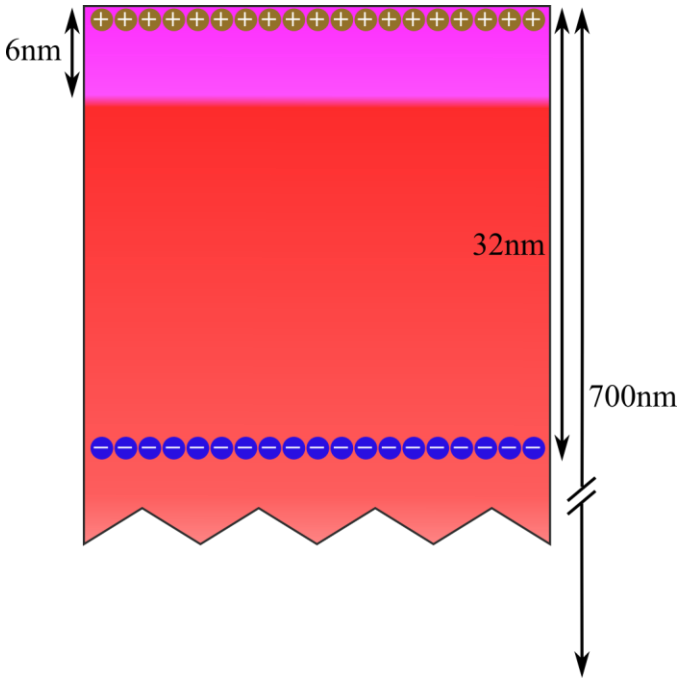

Fig. S6. Relative extents of the optical pulse penetration depths and the depletion width of the surface space charge region. The penetration depth of the 800nm pump and the 266nm probe pulses are approximately 700nm and 6nm respectively (*34*, *35*). The width of the depletion layer is estimated from the equation $w = \sqrt{\frac{2\varepsilon_0\varepsilon_r\phi_b}{qN_d}}$ (*33*) to be ~32nm at the sample surface, where ε_0 is the vacuum permittivity, ε_r is the relative permittivity, ϕ_b is the band bending at the surface, q is the electron charge and N_d is the dopant density. The narrow probing depth of the 266nm relative to the depletion width allows TR-PEEM to resolve the vertical transport of the photoexcited electrons due to the built-in surface field. With the much larger penetration depth of the 800nm pump compared to the depletion width, the carrier transport within the depletion region is largely determined by the surface field.

Movie S1. Gaussian electron distribution profile at low carrier density of 1.4×10^{18} cm^{-3}. At low carrier density, the distribution profile of the photoexcited electrons retains the Gaussian shape as the photocarriers diffuse and recombine over time.

Movie S2. Redistribution of the photoexcited electrons at 2.1×10^{19} cm^{-3}. The formation of local lateral electric fields generated using ultrafast light pulls apart the photoexcited electrons leading to the eventual separation of the photoexcited electrons into two distinct distributions. Each frame showing the photoexcited carrier distribution is normalized individually.